NASA/TM—2003-212390

$CuInS_2$ Films Deposited by Aerosol-Assisted Chemical Vapor Deposition Using Ternary Single-Source Precursors

Michael Jin
Ohio Aerospace Institute, Brook Park, Ohio

Kal Banger and Jerry Harris
Cleveland State University, Cleveland, Ohio

Aloysius Hepp
Glenn Research Center, Cleveland, Ohio

September 2003

The NASA STI Program Office . . . in Profile

Since its founding, NASA has been dedicated to the advancement of aeronautics and space science. The NASA Scientific and Technical Information (STI) Program Office plays a key part in helping NASA maintain this important role.

The NASA STI Program Office is operated by Langley Research Center, the Lead Center for NASA's scientific and technical information. The NASA STI Program Office provides access to the NASA STI Database, the largest collection of aeronautical and space science STI in the world. The Program Office is also NASA's institutional mechanism for disseminating the results of its research and development activities. These results are published by NASA in the NASA STI Report Series, which includes the following report types:

- TECHNICAL PUBLICATION. Reports of completed research or a major significant phase of research that present the results of NASA programs and include extensive data or theoretical analysis. Includes compilations of significant scientific and technical data and information deemed to be of continuing reference value. NASA's counterpart of peer-reviewed formal professional papers but has less stringent limitations on manuscript length and extent of graphic presentations.

- TECHNICAL MEMORANDUM. Scientific and technical findings that are preliminary or of specialized interest, e.g., quick release reports, working papers, and bibliographies that contain minimal annotation. Does not contain extensive analysis.

- CONTRACTOR REPORT. Scientific and technical findings by NASA-sponsored contractors and grantees.

- CONFERENCE PUBLICATION. Collected papers from scientific and technical conferences, symposia, seminars, or other meetings sponsored or cosponsored by NASA.

- SPECIAL PUBLICATION. Scientific, technical, or historical information from NASA programs, projects, and missions, often concerned with subjects having substantial public interest.

- TECHNICAL TRANSLATION. English-language translations of foreign scientific and technical material pertinent to NASA's mission.

Specialized services that complement the STI Program Office's diverse offerings include creating custom thesauri, building customized databases, organizing and publishing research results . . . even providing videos.

For more information about the NASA STI Program Office, see the following:

- Access the NASA STI Program Home Page at ***http://www.sti.nasa.gov***

- E-mail your question via the Internet to help@sti.nasa.gov

- Fax your question to the NASA Access Help Desk at 301–621–0134

- Telephone the NASA Access Help Desk at 301–621–0390

- Write to:
  NASA Access Help Desk
  NASA Center for AeroSpace Information
  7121 Standard Drive
  Hanover, MD 21076

NASA/TM—2003-212390

$CuInS_2$ Films Deposited by Aerosol-Assisted Chemical Vapor Deposition Using Ternary Single-Source Precursors

Michael Jin
Ohio Aerospace Institute, Brook Park, Ohio

Kal Banger and Jerry Harris
Cleveland State University, Cleveland, Ohio

Aloysius Hepp
Glenn Research Center, Cleveland, Ohio

National Aeronautics and
Space Administration

Glenn Research Center

September 2003

Acknowledgments

We gratefully acknowledge the National Aeronautics and Space Administration (NASA) for its support through grant, NCC3–947. The authors also wish to thank Mrs. Eunice Wong from the Electrochemistry Branch at NASA Glenn Research Center for her assistance with the Raman measurements.

Available from

NASA Center for Aerospace Information
7121 Standard Drive
Hanover, MD 21076

National Technical Information Service
5285 Port Royal Road
Springfield, VA 22100

Available electronically at http://gltrs.grc.nasa.gov

$CuInS_2$ Films Deposited by Aerosol-Assisted Chemical Vapor Deposition Using Ternary Single-Source Precursors

Michael Jin
Ohio Aerospace Institute
Brookpark, Ohio 44142

Kal Banger and Jerry Harris
Cleveland State University
Cleveland, Ohio 44115

Aloysius Hepp
National Aeronautics and Space Administration
Glenn Research Center
Cleveland, Ohio 44135

Abstract

Polycrystalline $CuInS_2$ films were deposited by aerosol-assisted chemical vapor deposition using both solid and liquid ternary single-source precursors (SSPs) which were prepared in-house. Films with either (112) or (204/220) preferred orientation, had a chalcopyrite structure, and (112)-oriented films contained more copper than (204/220)-oriented films. The preferred orientation of the film is likely related to the decomposition and reaction kinetics associated with the molecular structure of the precursors at the substrate. Interestingly, the (204/220)-oriented films were always In-rich and were accompanied by a secondary phase. From the results of post-growth annealing, etching experiments, and Raman spectroscopic data, the secondary phase was identified as an In-rich compound. On the contrary, (112)-oriented films were always obtained with a minimal amount of the secondary phase, and had a maximum grain size of about 0.5 μm. Electrical and optical properties of all the films grown were characterized. They all showed p-type conduction with an electrical resistivity between 0.1 and 30 Ω·cm, and an optical band gap of approximately 1.46 eV ± 0.02, as deposited. The material properties of deposited films revealed this methodology of using SSPs for fabricating chalcopyrite-based solar cells to be highly promising.

Photovoltaics are an important power source for both off-grid terrestrial and extraterrestrial use. Thin film polycrystalline materials have been studied extensively for solar cell applications partially because their polycrystalline nature allows their formation on many different types of substrates including glass, metal foil, and lightweight flexible polymer substrates.[1] For example, monolithically integrated $Cu(In,Ga)Se_2$ (CIGS) modules were recently realized on both metal foils and polymers with cell efficiencies up to 13.8 percent.[1] Using polymer substrates will particularly benefit space missions by reducing the power requirement for the payload of the spacecraft.[2] However, existing polymer substrates can only be processed under limited conditions because of their limited thermal durability. For example, Kapton™, a well-known space-qualified polymer material, can be processed at temperature up to 400 °C.

Previously we have developed new single-source precursors (SSPs) for chalcopyrite thin film formation.[3,4] One important prerequisite for SSPs is a lower decomposition temperature

than the substrate temperature so that film deposition can be initiated on polymer substrate without thermal degradation. It was successfully shown that SSPs' thermal properties were appropriate for a low-temperature process,[3,4] and film deposition using both solid and liquid SSPs in aerosol-assisted chemical vapor deposition (AACVD) reactors has been demonstrated.[5,6] AACVD is a useful alternative to conventional CVD when the vapor pressure of the precursor is too low for conventional CVD since it provides facile delivery of a precursor to a heated substrate by spraying it into a hot zone, followed by evaporation over a heated substrate.[7]

$CuInS_2$ is a wide band gap chalcopyrite, and it is a promising material for thin film solar cells because of its near optimum direct band gap of 1.5 eV, and its possible use as a top cell in a tandem structure with CIGS.[8] Although the best thin film solar cell efficiency reported was set by a CIGS heterojunction cell (18.8 percent) made at the National Renewable Energy Laboratory (NREL), $CuInS_2$ solar cells are theoretically expected to show efficiencies superior to those of CIGS cells.[9] However, total area efficiency of only 11.4 percent has been achieved thus far for $CuInS_2$ cells.[10]

In order to realize high performance CIGS and $CuInS_2$ solar cells, it is well understood that precise control of composition during film growth is critical because of the large number of possible intrinsic defects and their role in the dopant compensation, junction formation and carrier recombination.[8] In addition, a Cu-rich stage during the film growth is always necessary to achieve a large, columnar grain structure because the quasi-liquid Cu-S (or Se) binary phase segregated at the surface is believed to enhance the mobility of Cu and S (or Se) atoms during film growth.[11]

NREL's well-known 3-stage absorber layer growth[12] of world-record CIGS cells includes an In-rich stage (80 - 90 percent In and Ga) followed by the Cu-rich stage. In the final stage of the film growth, additional In and Ga (10 - 20 percent) are supplied to remove the Cu-Se binary phase. This In-rich surface is thought to have shallow donor states, which results in Fermi level pinning, and the subsequent type inversion from p-type to n-type.[8] The overall film composition also becomes In-rich.[8] This inverted surface is believed to minimize recombination at the interface between p-type CIGS and n-type CdS, which is the typical junction partner for CIGS.[8]

In contrast, the best $CuInS_2$ cell reported was made using a Cu-rich layer without an inverted In-rich surface,[10] even though the same advantage from the In-rich surface is expected. Surprisingly, forming the desirable inverted In-rich surface on top of Cu-rich film has not been accomplished for $CuInS_2$. Walter *et al*. tried a bilayer structure to realize an In-rich surface for $CuInS_2$,[13] and to our knowledge, there have been no further studies reported. Furthermore, the segregation of a spinel phase could occur very readily, even with slight deviations from stoichiometry on the In-rich side,[14] and In-rich $CuInS_2$ typically has a low carrier density ($\sim 10^{13}$ cm^{-3})[8] although the defect chemistry of $CuInS_2$ is known to be analogous to that of CIGS, and p-type In-rich CIGS can be made with a carrier density around 10^{17} cm^{-3}.[15]

It was reported that annealing In-rich films in a sulfur-rich atmosphere during an extended cool-down period enhanced the lateral conductivity at room temperature, and solar cell performance was significantly improved resulting in the highest efficiency (8.3 percent) for an In-rich $CuInS_2$ cell.[16] Systematic studies aimed at controlling the composition of the top surface during $CuInS_2$ film growth should be performed to achieve a single-phase In-rich surface with a hole density of $10^{17} \sim 10^{18}$ cm^{-3}, and enabling better heterojunction formation. In this study, we characterized structural, compositional, optical, and electrical properties of films deposited by AACVD using SSPs in order to establish a blueprint for a low-cost, low-temperature $CuInS_2$ thin

film deposition process for solar cells. The identification of phases and the study of film composition revealed a link between the film texture and a secondary phase formation.

Experimental

Previously reported $CuInS_2$ SSPs, $(PPh_3)_2CuIn(SEt)_4$ and $\{P(n\text{-}Bu)_3\}_2CuIn(SEt)_4$ were synthesized following a modified version of the procedure reported by Kanatzidis.[3,17] During the preparation, the thiol derivative was generated in situ by a reaction of the conjugate acid with NaOEt in methanol and produced no undesirable side products in addition to the 'activated' NaSEt. Because of their sensitivity to O_2 and H_2O, all reagents were handled in an argon-filled glove box (Vacuum Atmospheres Company). Both solid and liquid precursors were dissolved in toluene prior to atomization. Although the liquid precursor does not require any solvent in principle, the viscosity of the pure liquid precursor is too high to be atomized by the ultrasonic equipments used in this study. The viscosity of the liquid precursor, $\{P(n\text{-}Bu)_3\}_2CuIn(SEt)_4$ is about 340 ± 60 cp, and the upper viscosity limit for the atomizer used is on the order of 50 cp.

AACVD was performed in three different configurations. The first reactor is a horizontal atmospheric pressure hot-wall reactor (reactor A) with a plate-type ultrasonic nebulizer (Sonaer Ultrasonics, 2.5 MHz). The second reactor is a vertical atmospheric pressure cold-wall reactor (reactor B) with a commercial ultrasonic nozzle (Sono-Tek 120 kHz), and the third is a horizontal low-pressure hot-wall reactor (reactor C) with a pulsed aerosol injection system using a commercial automotive fuel-injector (Ford 2M2EA7B). Although they all share a common feature that precursor solution is delivered to the heated substrate as a form of sprayed aerosol, each reactor has its own set of advantages. For example, a cold-wall reactor (B) can minimize unnecessary decomposition of the precursor solution before it reaches the substrate. Pulsed aerosol injection at low pressure (C) allows film growth to occur at more well-defined conditions than a continuous process because undesirable transient effects due to highly volatile solvents can be minimized.[18] The description of the deposition processes for five representative films (film I, II, III, IV, and V) is summarized in Table I, and a detailed film growth process with schematics of the reactors can be found elsewhere.[5,6] Glass slides (Corning 2947 and 7059) and molybdenum coated slides were typically used as the substrate. Molybdenum was deposited by radio-frequency magnetic sputtering (Materials Research Corporation), and commercial Mo foil substrates were also used.

The viscosity of the liquid precursor was measured by a digital viscometer (Brookfield DV-I+), and film thickness was measured by a high-resolution profilometer (KLA-Tencor HRP 75). X-ray diffraction (XRD) (Philips) was used for phase identification, and glancing angle X-ray diffraction (GAXRD) was also performed using the same instrument to identify phases on the surface of films. Film morphology was examined using scanning electron microscopes (Hitachi S-3000N and S-800), and the composition of the films was analyzed by energy dispersive spectroscopy (EDS) (EDAX) built into the Hitachi S-3000N. The Cu/In ratio was calculated by quantifying Cu K and In L lines by the ZAF standardless method. Data was collected several times at different positions within each sample to minimize error. Further structural characterization was performed using an Almega dispersive Raman spectrometer (Thermo Nicolet). The optical bandgap was determined by analyzing optical transmittance measured using a UV-VIS spectrophotometer (Perkin-Elmer Lamda-19), and electrical measurements were performed using both a four-point probe system (Bio-Rad HL5500PC)

operated in the Van der Pauw configuration, and a custom hot-point probe – a commercial soldering iron (Weller TC201) was used as the hot probe.

Results and Discussion

Figure 1 exhibits the representative SEM pictures showing the grain morphology of films deposited in the three different reactors. Dense and columnar grain growth was realized with the hot-wall reactors. Figure 1(a) shows an example of the columnar grain structure (Film I), which is desirable because photo-excited carriers can easily recombine at grain boundaries, and a vertical columnar grain structure can lower the cross section of the recombination.

In contrast, figures 1(b) obtained from film III, grown with the cold-wall reactor B, did not show columnar grains but a porous nano-structure. Each particle (cluster) observed under low magnification, is actually comprised of smaller nanoparticles (~ 100 nm) that are clearly revealed with high magnification (inset of figure 1(b)). It was believed that the nanoparticles were created over the hot substrate by pyrolysis of nano-drops generated from the aerosol that continued carrying the ultrasonic excitation and further broke into a number of substructures.[19] Using the previously reported model,[19] the size of nanoparticles was estimated to be about 100 nm, assuming an average aerosol droplet diameter of 13 μm, as determined by theoretical prediction.[20,21] Clusters could be formed by the coagulation of nanoparticles before landing on the growth surface.[22] Although the observed nanoparticle size is in good agreement with theory, other variables should also be considered. First, can nanoparticles hold their integrity as a film by sintering? Although it is well known that the melting temperature of nano-clusters is much lower than that of bulk material,[23] the substrate temperature was 500 °C at most. Secondly, partial evaporation of the liquid droplet can cause grain growth under liquid deposition instead of vapor deposition, and the liquid deposition can yield nano-structured porous films. This growth mechanism was recently discussed in great detail,[6] and is beyond the scope of this paper.

Films IV and V grown with reactor C had representative grain structures that we have often observed throughout this study. The dendritic microstructure (film IV, figure 1(c)) showed non-faceted and elongated grains, which were also observed in films grown with solid SSPs in reactor A.[5] This was studied previously, and it was concluded to be a consequence of diffusion-limited growth.[24] By increasing the flow rate, dense and faceted trigonal-shaped grains were obtained (film V, figure 1(d)). The intersection of {211} faces in the chalcopyrite structure creates the trigonal-shaped grains. Grain size was about 0.5 μm. It was the largest grain size we have achieved so far using SSPs.

XRD patterns (figure 2(a)) showed that the films were either (112) or (204/220) preferentially oriented and they most likely had a chalcopyrite structure. The distinction between chalcopyrite and spharelite, a high temperature phase of chalcopyrite is often made by differences in their XRD patterns.[25] One difference is the splitting of some of the peaks associated with equivalent planes in spharelite, which correspond to different planes in chalcopyrite. This splitting appeared to be very weak but present for the films grown in this study. Because all other peaks observed in the XRD patterns are allowed both in chalcopyrite and spharelite, the patterns could not be used further to identify phases. Accordingly films appear to be a mixture of chalcopyrite and spharelite. In addition, films often contained a secondary phase ($2\theta \cong 26.5°$ in figure 2). A peak located near the same 2θ position was previously observed when either In-rich or S-rich solutions were used for spray pyrolysis, and it was identified as a $C_3H_4Cl_2N_6$ phase.[26] However, the $C_3H_4Cl_2N_6$ phase can not be responsible

for the peak observed in this study because SSPs do not produce by-products which can form the phase. A recent study also could not assign the same reflection at 26.5 ° to any phase, but found that it was characteristic for In-rich films.[27]

One unique aspect we consistently observed in this study was that the more the film is (204/220)-oriented, the more likely the film contains the secondary phase (figure 2(a)). Previous studies on the same type of SSPs also showed this trend although it was not examined.[26,28] Contreras *et al*. reported that there is an equivalent symmetry between the {100} plane of γ-In_2Se_3 (hexagonal) and the {102} plane of $CuInSe_2$, and γ-In_2Se_3 can be a precursor layer of (204)-oriented $CuInSe_2$.[29]

Although it is premature to conclude that the secondary phase observed is γ-In_2S_3, it is conclusive that the secondary phase is an as yet unidentified In-rich compound (either binary or ternary phase) because EDS measurements (figure 3) revealed in the films containing the secondary phase were always slightly In-rich, and an increase in the Cu/In ratio was generally observed when the secondary phase was removed upon annealing (figures 2(b) and 3). The GAXRD pattern (figure 2(c)) shows that the secondary phase is concentrated at the surface, and several films containing the secondary phase were etched in a 10 percent aqueous KCN solution for
2 min, which is a typical etch recipe to remove a copper sulfide phase segregated to the surface of $CuInS_2$.[30] XRD confirmed the secondary phase was not removed by the solution in all films. If the secondary phase was the copper sulfide phase, it should be easily etched away by the solution since the etch rate of Cu-rich phases in KCN solutions is much higher than that of In-rich phases.[30]

Further correlation between the secondary phase and the In-rich environment was confirmed by Raman spectroscopy (figure 4). We observed that the spectrum showed a very strong mode at 305 cm^{-1} when the film was In-rich, (204/220)-oriented, and contained a significant amount of the secondary phase. However, the mode was less prominent when the film was slightly Cu-rich and (112)-oriented. It was reported that this additional mode could be assigned to a defect-related In-rich local vibrational mode.[25,31] The In-rich secondary phase could originate from this In-rich local environment. However, alternate ordering of Cu and In on the (201) planes of metal sublattice (Cu-Au ordering) was found in polycrystalline $CuInS_2$ films,[32] and this ordering could also be the origin of the mode. Further discussion about this mode can be found in the literature.[31]

In order to prevent secondary phase formation, (112)-oriented film growth must be targeted, and the surface kinetic regime where (204/220)-oriented film growth is favored, should be avoided. It is known that the molecular structure and the decomposition kinetics of the precursor at the growth surface can affect the overall surface kinetics and subsequent film growth, resulting in a different preferred orientation.[33] By exploring different growth process parameters, we have succeeded in growing (112)-oriented films without observing the In-rich secondary phase in the XRD (figure 2(a), Film V). The Cu/In ratio was measured from 10 different locations on the film by EDS, and it was slightly Cu-rich (1.08 ± 0.06). Meanwhile, it was not possible, within our experimental space, to grow (204/220)-oriented film without the secondary phase although the phase can be easily removed by post-growth heat treatment (figure 2(b)). It should be noted that some possible advantages of (204/220)-oriented $CuInSe_2$ film over (112)-oriented film were previously addressed.[34] However, having the secondary phase in the absorber layer is not desirable, and this excludes the use of (204/220)-oriented films as grown using the SSPs.

Achieving larger grain size should take precedence in future studies because the grain size as grown is too small for absorber layer use in solar cells. As mentioned earlier, the copper sulfide phase naturally or intentionally incorporated into $CuInS_2$ facilitates larger grain growth. In fact, most of films we have grown were near stoichiometric, being slightly In- or Cu-rich, and have never shown any sign of a copper sulfide phase. Overcoming this will provide the footage for a promising future for $CuInS_2$ SSPs.

The band gap of films was estimated from the plot of $(\alpha \cdot E)^2$ versus E, where α is an absorption coefficient estimated from the optical transmittance data and E is photon energy (figure 5).[35] Band gap energies ranging between 1.45 eV and 1.47 eV were obtained from films grown in this study. The figure shows that the band edge sharpens upon post-growth annealing, which is ascribed to improved crystallinity and densification (film III). However, the overall change of the absorption curve, including the shift of the band gap after annealing, was complicated by the removal of the secondary phase. The optical transition related to the secondary phase was sought, but results were not conclusive. The overall absorption of film V was higher than that of film III in the figure, and this was attributed to the difference in the density between the two films; film V had a denser grain structure than film III as shown in figure 1.

All films grown using the three different reactors showed p-type conduction regardless of composition and morphology. A hot-point probe was routinely tested with reference n- and p-type materials before measurement to validate the results. Bulk resistivity was calculated by multiplying sheet resistance with measured thickness, and it ranged from 0.1 Ω·cm to 30 Ω·cm. Although Cu-rich films showed lower resistivities than In-rich films, further studies of defect formation and compensation between defects, are required to make a more definitive correlation. It should be noted, however that the lowest resistivity reported for a $CuInS_2$ film prepared by spray pyrolysis, was 0.1 Ω·cm (carrier concentration of 10^{18} cm^{-3}), and a solution containing up to 30 percent excess copper was used.[36]

Conclusions

The correlation between the texture and the composition of $CuInS_2$ films deposited by AACVD using SSPs was studied. The (112)-oriented films deposited without a signature of a secondary phase were slightly Cu-rich. The (204/220)-oriented films were In-rich and always included the secondary phase. The secondary phase was further thought to be an In-rich compound because it was not etched away by KCN treatment, and the Raman spectra of (204/220)-oriented films always showed the strong 305 cm^{-1} mode, which can originate from an In-rich environment.[25,31] In addition, the Cu/In ratio of the film increased by removing the secondary phase through post-growth annealing at 600 °C. The bulk resistivity calculated from sheet resistance was between 0.1 Ω·cm and 30 Ω·cm, and p-type conduction was observed for all the $CuInS_2$ films grown using SSPs. A typical band gap of 1.46 eV ± 0.02 was measured. Although possible single-phase chalcopyrite $CuInS_2$ films with a dense columnar grain structure were obtained by depositing (112)-oriented films, the grain size was small (≤ 0.5 μm) due to the absence of a quasi-liquid Cu binary phase. The possible composition of the film was limited due to the built-in stoichiometry in the SSPs. Further development is necessary to grow films with higher Cu concentrations to obtain bigger grains suitable for solar cell applications.

References

1. F. Kessler, K. Herz, M. Powalla, M. Hartmann, M. Schmidt, A. Jasenek, and H. W. Schock, Mat. Res. Soc. Symp. Proc. **668**, H3.6.1 (2001).
2. G. A. Landis and A. F. Hepp, *Proceedings of European Space Power Conference,* ESA SP–320, 517 (1991).
3. K. K. Banger, J. Cowen, and A. F. Hepp, *Chem. Mater.*, **13**, 3827 (2001).
4. K. K. Banger, J. D. Harris, J. E. Cowen, A. F. Hepp, *Thin Solid Films*, **403–404**, 390 (2002).
5. J. D. Harris, D. G. Hehemann, J. E. Cowen, A. F. Hepp, R. P. Raffaelle, and J. A. Hollingsworth, *Proceedings of the 28th IEEE Photovoltaic Specialists Conference,* 563 (2000).
6. M. H.-C. Jin, K. K. Banger, J. D. Harris, J. E. Cowen, and A. F. Hepp, *29th IEEE Photovoltaic Specialists Conference,* 672 (2002).
7. T. T. Kodas and M. J. Hampden-Smith, *The Chemistry of Metal CVD*, p. 460, VCH, Weinheim (1994).
8. M. D. Archer and R. Hill, *Clean Electricity From Photovoltaics*, Chapter 7, Imperial College Press, Singapore (2001).
9. M. A. Contreras, B. Egaas, K. Ramanathan, J. Hiltner, A. Swartzlander, F. Hasoon, and R. Noufi, *Prog. Photovoltaic Res. Appl*., **7**, 311 (1999).
10. J. Klaer, J. Bruns, R. Henninger, K. Töpper, R. Klenk, K. Ellmer, and D. Bräunig, *Proceedings of the 2nd World Conference on Photovoltaic Energy Conversion*, 537 (1998).
11. R. Klenk, T. Walter, H. W. Schock, and D. Cahen, *Adv. Mater*., **5**, 114 (1993).
12. M. A. Contreras, J. Tuttle, A. Gabor, A. Tennant, K. Ramanathan, S. Asher, A. Franz, J. Keane, L. Wang, J. Scofield, and R. Nouli, *Proceedings of the first World Conference on Photovoltaic Energy Conversion*, 68 (1994).
13. T. Walter, A. Content, K. O. Velthaus, and H. W. Schock, *Sol. Energy. Mater. Sol. Cells*, **26**, 357 (1992).
14. T. Walter and H. W. Schock, *Jpn. J. Appl. Phys*., **32–3**, 116 (1993).
15. S. Siebentritt, *Thin Solid Films*, **403-404**, 1 (2002).
16 R. Scheer, M. Alt, I. Luck, H. J. Lewerenz, *Sol. Energy. Mater. Sol. Cells*, **49**, 423 (1997).
17. W. Hirpo, S. Dhingra, A. C. Sutorik, and M. G. Kanatzidis, *J. Am. Chem. Soc*., **115**, 1597 (1993).
18. S. Krumdieck, O. Sbaizero and R. Raj, *J. Phys. IV*, **11**, Pr3–1161 (2001).
19. V. Jokanovic, Dj. Janackovic, P. Spasic, and D. Uskokovic, *Nanostruct. Mater*., **12**, 349 (1999).
20. R. J. Lang, *J. Acoust. Soc. Am*., **34**, 6 (1962).
21. Dj. Janackovic, V. Jokanovic, Lj. Kostic-Gvozdenovic, and D. Uskokovic, *Nanostruct. Mater*., **10**, 341 (1998).
22. T. T. Kodas and M. J. Hampden-Smith, *Aerosol Processing of Materials*, Chapter 5, WILEY-VCH, New York (1999).
23. C. C. Koch, *Nanostructured Materials*, p. 227, Noyes publications, Norwich (2002).
24. J. A. Hollingsworth, A. F. Hepp, and W. E. Buhro, *Chem. Vap. Deposition*, **5**, 105 (1999).
25. J. Álvarez-García, A. Pérez-Rodríguez, A. Romano-Rodríguez, J. R. Morante, L. Calvo-Barrio, R. Scheer, and R. Klenk, *J. Vac. Sci. Technol. A*, **19**, 232 (2001).
26. M. Krunks, V. Mikli, O. Bijakina, H. Rebane, A. Mere, T. Varema, and E. Mellikov, *Thin Solid Films*, **361–362**, 61 (2000).

27. I. V. Luck, J. Alvarez-Garcia, L. Calvo-Barrio, A. Werner, A. Perez-Rodriguez, J. R. Morante, and D. Bräunig, Mat. Res. Soc. Symp. Proc. **668**, H1.4.1 (2001).
28. R. Mu, D. O. Henderson, A. Ueda, M. H. Wu, J. A. Bennett, M. A. M. Paliza, M. B. Huang, J. Keay, L. C. Feldman, K. C. Kwiatkowski, C. M. Lukehart, J. Hollingsworth, W. E. Buhro, J. Harris, E. Gordon, and A. Hepp, *Proceeding of the SPIE Conference on Solar Optical Materials XVI*, **3789**, 116 (1999).
29. M. A. Contreras, B. Egaas, D. King, A. Swartzlander, and T. Dullweber, *Thin Solid Films*, **361–362**, 167 (2000).
30. M. Weber, R. Scheer, H. J. Lewerenz, H. Jungblut, and U. Störkel, *J. Electrochem. Soc.*, **149**, G77 (2002).
31. J. Álvarez-García, A. Pérez-Rodríguez, A. Romano-Rodríguez, T. Jawhari, J. R. Morante, R. Scheer, and W. Calvet, *Thin Solid Films,* **387**, 216 (2001).
32. D. S. Su, W. Neumann, and M. Giersig, *Thin Solid Films*, **361–362**, 218 (2000).
33. A. N. MacInnes, M. B. Power, and A. R. Barron, *Chem. Mater*., **5**, 1344 (1993).
34. D. Liao and A. Rockett, *Proceedings of the 28th IEEE Photovoltaic Specialists Conference, 446* (2000).
35. M. Krunks, O. Bijakina, T. Varema, V. Mikli, E. Mellikov, *Thin Solid Films*, **338**, 125 (1999).
36. A. N. Tiwari, D. K. Pandya, and K. L. Chopra, *Thin Solid Films*, **130**, 217 (1985).

Table I.—Selected aerosol-assisted deposition processes for $CuInS_2$ films

Film	I	II	III	IV	V
Reactor	A	A	B	C	C
Precursor	solid	solid	liquid	liquid	liquid
Precursor concentration (M)	0.01	0.01	0.01	0.01	0.01
Precursor delivery method	gravity-driven	gravity-driven	syringe pump	vacuum-driven	vacuum-driven
Precursor delivery rate (ml/min)	~ 1.7	~ 1.7	1.5	0.4	0.4
Temperatures (ºC)					
zone 1:	128	120	no zones	250	150
zone 2:	390	360		250	250
substrate:	390[#]	360[#]	400	420	400
Pressure (torr)	atm.	atm.	atm.	~ 12	~ 10
Ar flow rate (l/min)	4	4	4	0.08[*]	0.15[*]
Substrate	Mo/glass (Corning 2947)	Mo foil	glass (Corning 7059)	Mo/glass (Corning 2947)	Mo/glass (Corning 2947)
Growth time (min)	80	60	60	250	250
Thickness (μm)	~ 1	~ 1	~ 4	~ 1	~ 1

Solid precursor: $(PPh_3)_2CuIn(SEt)_4$
Liquid precursor: $\{P(n\text{-}Bu)_3\}_2CuIn(SEt)_4$
[#]Substrate is located within the zone 2. There is no direct substrate heating.
[*]Direct reading from MKS flow controller (not calibrated).

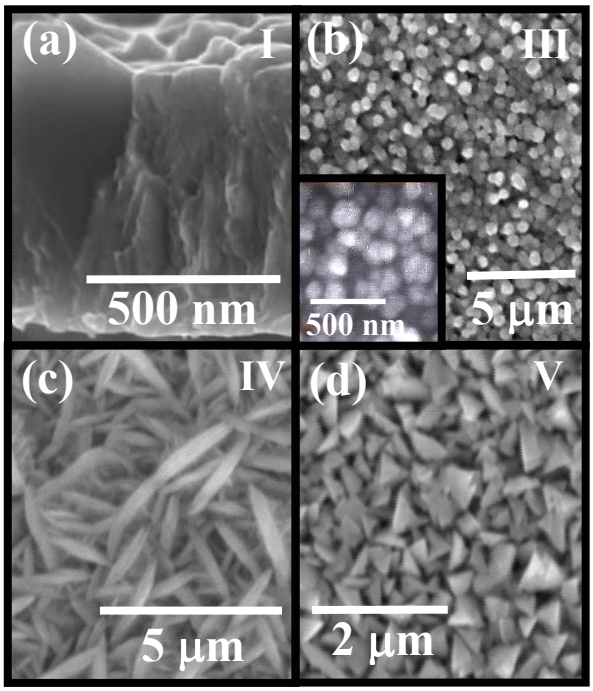

Figure 1 SEM micrographs of $CuInS_2$ films grown by aerosol-assisted chemical vapor deposition: (a) the cross-section image of film I, (b) the plane-view of image of fill III with a high magnification image as an inset (c) the plane-view image of film IV, and (d) the plane-view image of film V.

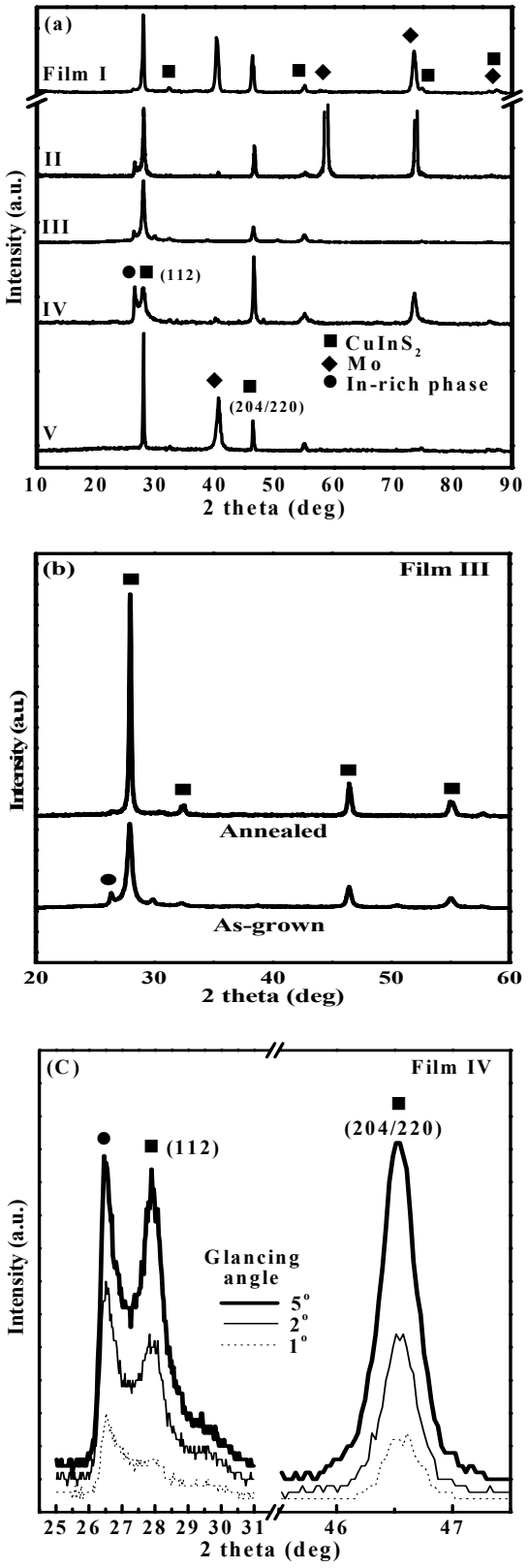

Figure 2 XRD spectra of $CuInS_2$ films grown by aerosol-assisted chemical vapor deposition: (a) untreated films, (b) film III with a post-growth heat treatment, and (c) glancing angle XRD spectrum of film IV.

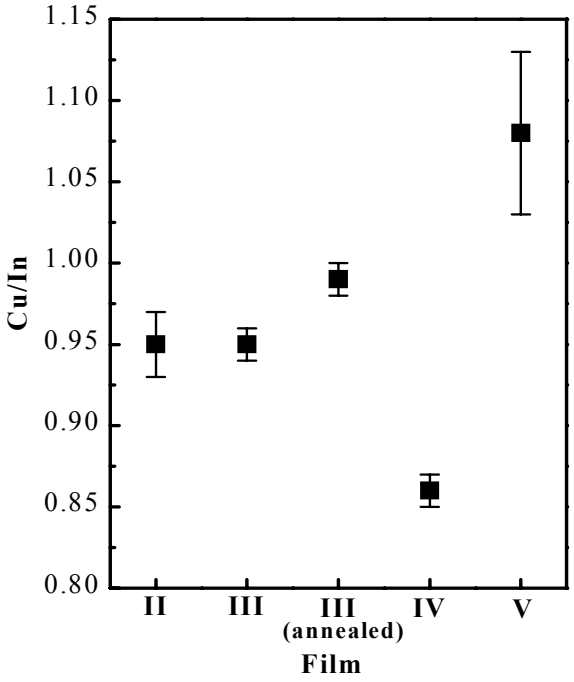

Figure 3 Cu/In ratio of $CuInS_2$ films determined from electron dispersive spectroscopy.

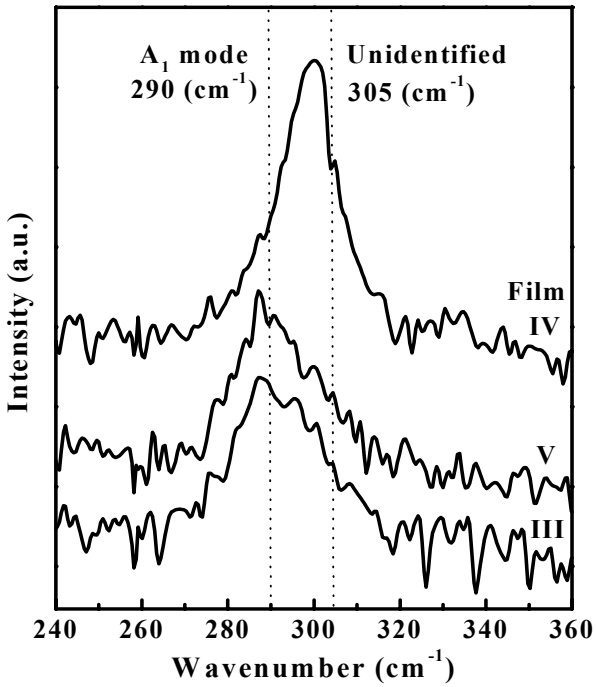

Figure 4 Raman spectra of $CuInS_2$ films III, IV, and V.

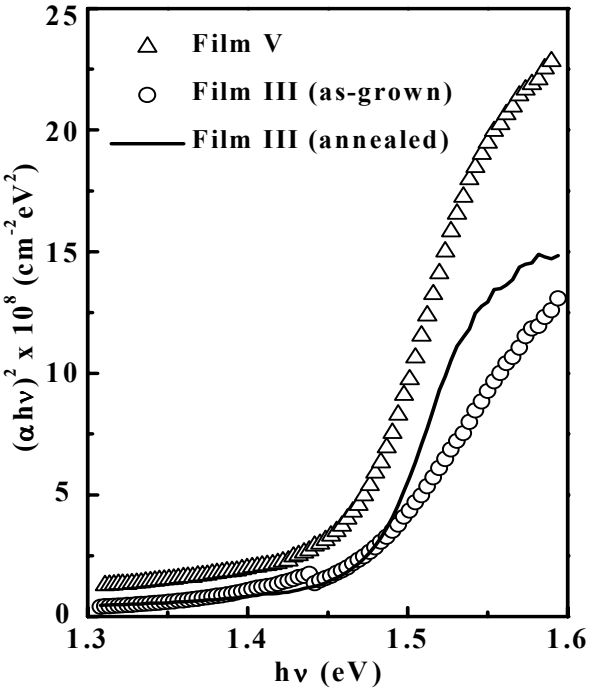

Figure 5 A plot of $(\alpha \cdot E)^2$ versus E for the $CuInS_2$ films, III and V.

REPORT DOCUMENTATION PAGE

Form Approved
OMB No. 0704-0188

1. AGENCY USE ONLY (*Leave blank*)	2. REPORT DATE	3. REPORT TYPE AND DATES COVERED
	September 2003	Technical Memorandum

4. TITLE AND SUBTITLE

$CuInS_2$ Films Deposited by Aerosol-Assisted Chemical Vapor Deposition Using Ternary Single-Source Precursors

5. FUNDING NUMBERS

WBS–22–755–60–01

6. AUTHOR(S)

Michael Jin, Kal Banger, Jerry Harris, and Aloysius Hepp

7. PERFORMING ORGANIZATION NAME(S) AND ADDRESS(ES)

National Aeronautics and Space Administration
John H. Glenn Research Center at Lewis Field
Cleveland, Ohio 44135–3191

8. PERFORMING ORGANIZATION REPORT NUMBER

E–13967

9. SPONSORING/MONITORING AGENCY NAME(S) AND ADDRESS(ES)

National Aeronautics and Space Administration
Washington, DC 20546–0001

10. SPONSORING/MONITORING AGENCY REPORT NUMBER

NASA TM—2003-212390

11. SUPPLEMENTARY NOTES

Michael Jin, Ohio Aerospace Institute, Brook Park, Ohio 44142; Kal Banger and Jerry Harris, Cleveland State University, Cleveland, Ohio 44115; and Aloysius Hepp, NASA Glenn Research Center. Responsible person, Aloysius Hepp, organization code 5410, 216–433–3835.

12a. DISTRIBUTION/AVAILABILITY STATEMENT

Unclassified - Unlimited
Subject Categories: 23, 33, and 44 Distribution: Nonstandard

Available electronically at http://gltrs.grc.nasa.gov

This publication is available from the NASA Center for AeroSpace Information, 301–621–0390.

12b. DISTRIBUTION CODE

13. ABSTRACT ***(Maximum 200 words)***

Polycrystalline $CuInS_2$ films were deposited by aerosol-assisted chemical vapor deposition using both solid and liquid ternary single-source precursors (SSPs) which were prepared in-house. Films with either (112) or (204/220) preferred orientation, had a chalcopyrite structure, and (112)-oriented films contained more copper than (204/220)-oriented films. The preferred orientation of the film is likely related to the decomposition and reaction kinetics associated with the molecular structure of the precursors at the substrate. Interestingly, the (204/220)-oriented films were always In-rich and were accompanied by a secondary phase. From the results of post-growth annealing, etching experiments, and Raman spectroscopic data, the secondary phase was identified as an In-rich compound. On the contrary, (112)-oriented films were always obtained with a minimal amount of the secondary phase, and had a maximum grain size of about 0.5 μm. Electrical and optical properties of all the films grown were characterized. They all showed p-type conduction with an electrical resistivity between 0.1 and 30 Ω·cm, and an optical band gap of approximately 1.46 eV ± 0.02, as deposited. The material properties of deposited films revealed this methodology of using SSPs for fabricating chalcopyrite-based solar cells to be highly promising.

14. SUBJECT TERMS

Energy conversion; Solar cells; $CuInS_2$; Spray pyrolysts; Single source precursors

15. NUMBER OF PAGES

18

16. PRICE CODE

17. SECURITY CLASSIFICATION OF REPORT	18. SECURITY CLASSIFICATION OF THIS PAGE	19. SECURITY CLASSIFICATION OF ABSTRACT	20. LIMITATION OF ABSTRACT
Unclassified	Unclassified	Unclassified	